JPE 18-2-14

https://doi.org/10.6113/JPE.2018.18.2.467
ISSN(Print): 1598-2092 / ISSN(Online): 2093-4718

Advanced Small-Signal Model of Multi-Terminal Modular Multilevel Converters for Power Systems Based on Dynamic Phasors

Pan Hu†, Hongkun Chen*, Lei Chen*, Xiaohang Zhu*, and Xuechun Wang*

†,*School of Electrical Engineering, Wuhan University, Wuhan, China

Abstract

Modular multilevel converter (MMC)-based high-voltage direct current (HVDC) presents attractive technical advantages and contributes to enhanced system operation and reduced oscillation damping in dynamic MMC–HVDC systems. We propose an advanced small-signal multi-terminal MMC–HVDC based on dynamic phasors and state space for power system stability analysis to enhance computational accuracy and reduce simulation time. In accordance with active and passive network control strategies for multi-terminal MMC–HVDC, the matchable small-signal stability models containing high harmonics and dynamics of internal variables are conducted, and a related theoretical derivation is carried out. The proposed advanced small-signal model is then compared with electromagnetic–transient and traditional small-signal state-space models by adopting a typical multi-terminal MMC–HVDC network with offshore wind generation. Simulation indicates that the advanced small-signal model can successfully follow the electromechanical transient response with small errors and can predict the damped oscillations. The validity and applicability of the proposed model are effectively confirmed.

Key words: Advanced small-signal model, Dynamic phasors, Multi-terminal MMC–HVDC, Power system stability

NOMENCLATURE

Subscripts q, d	q-axis and d-axis components of the variable
Subscript s	AC side index
Subscript c	Side index before the MMC–HVDC valve
Subscript j	Phase index = {a, b, c}
Subscripts p, n	Upper and lower variables in phase
Subscript i	Integer index = {1, 2, 3, ……}
Subscript cir	2nd harmonic circulation component
Superscript $*$	Conjugate of the complex
L_0, R_0	Equivalent inductor and resistor per arm
C	Capacitance of one SM
U_{dc}, I_{dc}	DC voltage and current of MMC–HVDC
u_{dc_ac1}, u_{dc_ac2}, u_{dc_ac3}	1st, 2nd, and 3rd AC voltage fluctuation
$\overline{u_c}$	DC voltage component
$\overline{P_{dc}}$	Total DC power fluctuations of capacitance in the arm
L_i, R_i	Equivalent AC inductance and resistance
i_{sdi}^*, i_{sqi}^*	d-axis and q-axis reference inner current
θ_0	Voltage phase angle of U_s
θ_{PLL}	Voltage phase angle of PLL
k_{pi*}, k_{ii*}	Proportional and integral gains of the dual loop
k_{cirp*}, k_{ciri*}	Proportional and integral gains of circle suppression
$k_{\theta p}$, $k_{\theta i}$	Proportional and integral gains of PLL
$X_k(t)$	k-th harmonic Fourier coefficient

Manuscript received Jun. 14, 2017; accepted Nov. 27, 2017
Recommended for publication by Associate Editor Kai Sun.
†Corresponding Author: 314784284@qq.com
Tel: +86-027-6877-3898, Fax: +86-027-6877-3898, Wuhan University
*School of Electrical Engineering, Wuhan University, China

I. INTRODUCTION

Given the continuous development of modern electrical power networks and power electronics, the HVDC transmission system is currently considered one of the main components of

future network configurations [1]-[3]. Compared with traditional HVDC links, MMC–HVDC has greater controllability and flexibility and presents more technical advantages [4], [5]. MMC–HVDC could be used to address challenges associated with the interconnection of large geographical AC networks and renewable energy resources. Investigating the stability of power systems that contain multi-terminal MMC–HVDC by establishing matchable small-signal models is valuable and meaningful.

Researchers have conducted a few studies on small-signal models of voltage source converter-based HVDC (VSC–HVDC) and MMC–HVDC [6]-[12]. In [6] and [7], a small-signal model of a hybrid network comprising VSC–HVDC and traditional AC transmission was discussed to investigate low-frequency electromechanical oscillation and analyze the DC dynamics of multi-terminal systems. In [8], a small-signal model of multi-terminal VSC-based DC systems was established for the analysis of control parameters. However, this model does not consider the effect of a phase-locked loop (PLL) controller, and its suitability should be improved further. A unified model of multi-terminal VSC-HVDC systems was built in [9] by utilizing power injections and linearized elements to conduct hybrid flow calculations. In [10], a generic root-mean-square (RMS) model was proposed for the study of MMC–HVDC on the basis of existing averaged models. Although these models exhibit an acceptable dynamic performance, their steady-state errors can still be reduced through technological improvement. Two simplified MMC–HVDC state-space models for electromechanical transient analyses were established in [11] and [12], and both can reduce simulation time to a certain extent. However, the application of these models in passive HVDC systems can still be improved because the effect of passive system controllers is not considered in the models.

These small-signal models are based on the quasi-steady state assumption, which ignores the dynamic process of the converter; moreover, the accuracy of electronic devices is lacking, and the fast electromagnetic process of systems is not accurately reflected [13]. Although the accuracy of electromagnetic–transient (EMT) models of systems and power electronic devices is high, the scale of networks significantly limits the calculation speed and complexity of computational simulations. For these cases, the generalized average dynamic phasor model can be utilized to explore the dynamics of power-electronic based systems by developing a low-intensity model [14]. The dynamic phasor (dyn.phasor) method is suitable for studying high-frequency characteristics of a system, and it has been successfully utilized in the modeling of electrical components and analysis of power systems containing electronic devices [15]-[19]. An improved small-signal model containing internal dynamics was proposed in [20] by considering the internal harmonic component of sub-modules (SMs). In [21], a phasor format model was presented for the modeling of MMC–HVDC for power flow and parameter studies. The researchers in [22] modeled a traditional HVDC system by using dynamic phasors to investigate large-excursion transients caused by control actions or faults. However, these models are inconvenient when used in power system stability analyses, and their application can be improved further.

We propose an advanced small-signal model of a multi-terminal MMC–HVDC for power system stability analysis to effectively enhance computation accuracy and reduce simulation time. This model is based on the dynamic phasor method and state space. PLL and an active/passive network control strategy are considered. Instead of analyzing the detailed response of DC power fluctuation per SM, the proposed model presents the equivalent external characteristic of MMC–HVDC as a unified element with high accuracy, and this approach is convenient for power system interaction studies. In Section III, a typical four-terminal MMC–HVDC test network is built, and a theoretical model of MMC–HVDC is provided. The multi-terminal small-signal stability models are presented in Section IV. The mathematical theory of dynamic phasors and the matchable advances are proposed in Section V. Section VI compares the proposed advanced small-signal model with EMT and traditional small-signal state-space models. The conclusions are summarized, and future research directions are presented.

II. Model of the Multi-Terminal MMC–HVDC System

A. Description of the Multi-terminal MMC–HVDC Test Network

The demonstrated four-terminal MMC–HVDC system includes one offshore wind farm and three conventional power sources. Fig. 1 shows a schematic of this HVDC system. MMC1 and MMC4 are utilized to connect a weak active network and the wind farm through doubly fed induction generators (DFIGs). MMC2 and MMC3 are applied to two conventional power sources. AC network 2 has a high short-circuit ratio (SCR). The nominal operation state and parameters, such as power flow, control strategy, system impedances, and network SCR, are shown in Fig. 1.

B. Structure and Representation of the MMC–HVDC System

The EMT model structure of MMC–HVDC is shown in Fig. 2(a). Each phase is composed of two arms (up and down). Instead of providing a detailed description, the N submodules are represented as a controlled voltage source on each arm. For phase j ($j=a, b, c$), the averaged EMT model meets the following dynamic equation [21].

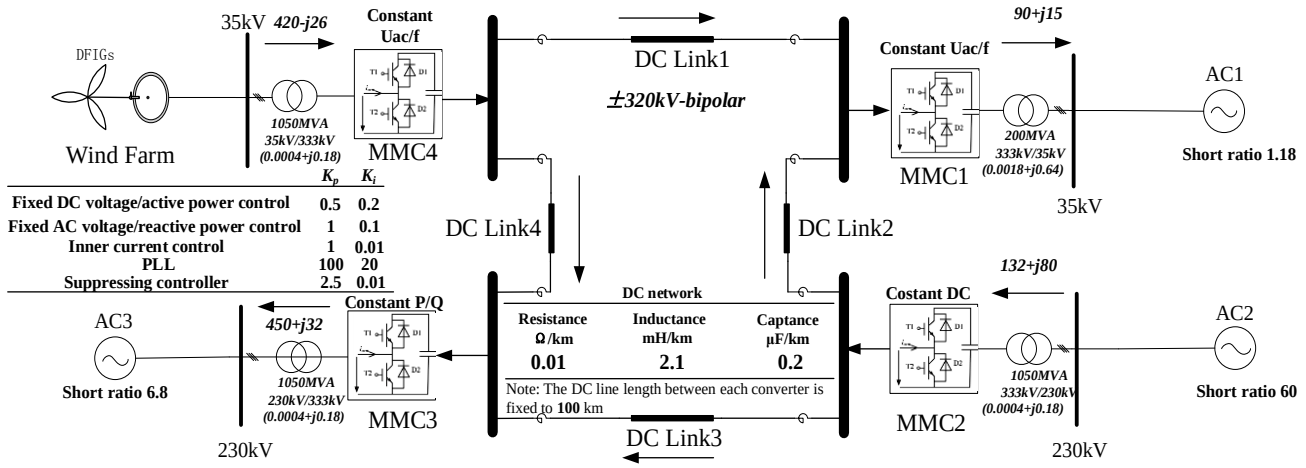

Fig. 1. Four-terminal MMC–HVCD test system.

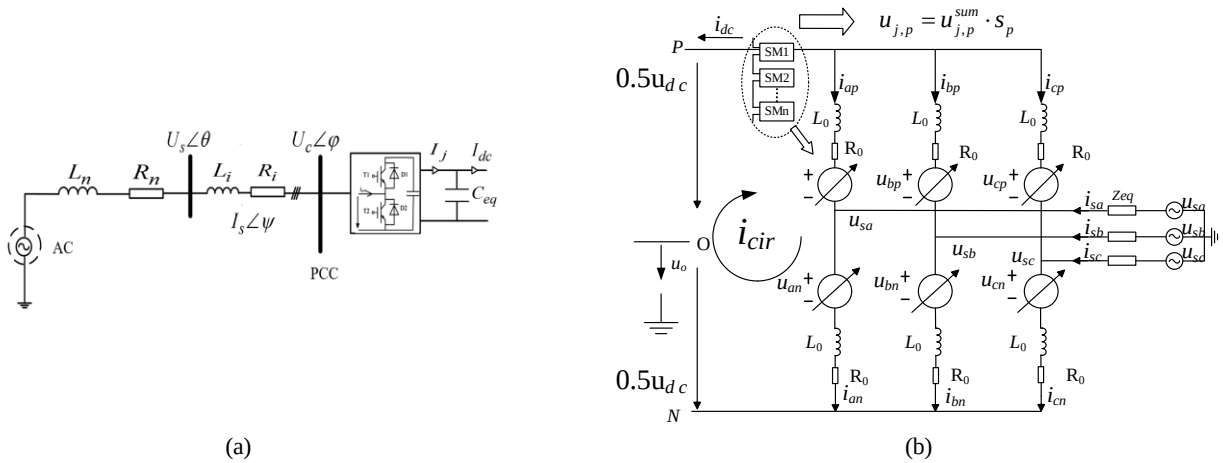

(a) (b)

Fig. 2. Topology of MMC–HVDC. (a) Structure of the converter and active network. (b) Averaged EMT model of MMC–HVDC.

$$\frac{d}{dt}\begin{bmatrix} i_{cir} \\ u^{sum}_{j,p} \\ u^{sum}_{j,n} \end{bmatrix} = \begin{bmatrix} -\frac{R_0}{L_0} & -\frac{S_p}{2} & \frac{S_n}{2} \\ -\frac{S_p}{C_0} & 0 & 0 \\ -\frac{S_n}{C_0} & 0 & 0 \end{bmatrix} \begin{bmatrix} i_{cir} \\ u^{sum}_{j,p} \\ u^{sum}_{j,n} \end{bmatrix} + \begin{bmatrix} -\frac{u_{dc}}{2} \\ -\frac{S_p i_{sj}}{2C_0} \\ \frac{S_n i_{sj}}{2C_0} \end{bmatrix}, \quad (1)$$

where $C_0 = C / N$ represents the capacitance of each arm. The switch function can be regarded as a continuous waveform due to the large number of SMs. By considering the second harmonic and DC element, S_p and S_n in Eq. (1) can be obtained as

$$\begin{cases} S_p = \frac{1}{2} - \frac{1}{2} M_1 \cos(\omega t + \varphi_1) - \frac{U_{cir}}{U_{dc}} \cos(2\omega t + \varphi_2) \\ \quad = \frac{1}{2} - \frac{1}{2}(M_{1d} \cos\omega t + M_{1q} \cos\omega t + M_{2d} \cos 2\omega t + M_{2q} \cos 2\omega t) \\ S_n = \frac{1}{2} + \frac{1}{2} M_1 \cos(\omega t + \varphi_1) - \frac{U_{cir}}{U_{dc}} \cos(2\omega t + \varphi_2) \\ \quad = \frac{1}{2} + \frac{1}{2}(M_{1d} \cos\omega t + M_{1q} \cos\omega t - M_{2d} \cos 2\omega t - M_{2q} \cos 2\omega t) \end{cases}, \quad (2)$$

where φ_1 is a first-order phase of voltage and current and U_{cir} and φ_2 are the amplitude and phase of the second harmonic generated by circulating–suppressing controllers. The fundamental modulation ratio with the additional second-phasor component can be expressed as

$$\begin{aligned} M_1 &= \frac{U_{sj}}{U_{dc}/2} \quad 0 \le M_1 \le 1 \\ M_2 &= \frac{U_{cir}}{U_{dc}/2} \quad 0 \le M_2 \le 1 \end{aligned}. \quad (3)$$

(M_{1d} , M_{1q}) and (M_{2d} , M_{2q}) in Eq. (2) are corresponding *dq0* components under frame rotating frequency (ω_0 and $2\omega_0$).

By disregarding the potential drop of arm impedance, the combined mathematical model of each phase can be obtained as

$$\begin{cases} I_{j,p}(t) = \frac{1}{3} I_{dc} - \frac{1}{2} I_s(t) \sin(\omega t + \varphi_1) + I_{cir} \sin(2\omega t + \varphi_2) \\ I_{j,n}(t) = \frac{1}{3} I_{dc} + \frac{1}{2} I_s(t) \sin(\omega t + \varphi_1) + I_{cir} \sin(2\omega t + \varphi_2) \end{cases}. \quad (4)$$

By utilizing Eqs. (2), (3), and (4) and ignoring the part of high-order components, the DC voltage per SM can be expressed as

$$\begin{aligned} u_c &= \overline{U_{dc}} + U_{dc\_ac1} + U_{dc\_ac2} + U_{dc\_ac3} \\ &= \overline{u_{dc}} + u_1 \sin(\omega t + \delta_1) + u_2 \sin(2\omega t + \delta_2) + u_3 \sin(3\omega t + \delta_3) \end{aligned}, \quad (5)$$

where u_1, δ_1, u_2, δ_2, u_3, and δ_3 are the respective orders of voltage amplitude and phase and can be obtained from [23] and [24].

Given that MMC can generally introduce high flexibility and applicability to a power system, its capacitance is split into sub-modules. Difficulties arise in detailed analyses of the response of DC power fluctuation per SM. Given that stability analysis mainly considers the equivalent external characteristic of an element, the equivalent capacitance of MMC is deduced to investigate the DC power transmission process in an entire multi-terminal MMC and improve the convenience of stability analysis.

Each phase arm is mainly achieved by the charge and discharge of the sub-modules' capacitance because of the energy variation. The equivalent capacitance can be obtained by establishing an energy fluctuation equation between the capacitance and bridge arm. The fluctuation energy of the upper arm of each phase can be obtained in combination with Eq. (4) and by ignoring the high-frequency part.

$$\Delta W_{uj}(m) = \int_{x_1(m,\varphi)}^{x_2(m,\varphi)} P_{uj}(\omega t) d(\omega t) = \frac{\overline{P_{dc}}}{3w} m \left(1 - \frac{1}{m^2}\right)^{\frac{3}{2}} = \frac{2P_s}{3kw} \left(1 - \left(\frac{k\cos\varphi}{2}\right)^2\right)^{\frac{3}{2}}, \quad (6)$$

where x_1 and x_2 are the zero-crossing of phase changes from $\pi/2$ to $\pi/4$. $\overline{P_{dc}}\mathrm{G_r}\ \mathrm{C_p}(\lambda,\beta) = 47\%$is the total DC power of the capacitance of each upper arm, which meets $P_s = \overline{P_{dc}}/\cos\varphi$. The total energy fluctuations of MMC are written as $\Delta W_s = 6 \times \Delta W_{uj}$. Energy fluctuations in capacitance can be expressed as $\Delta W_c = \frac{1}{2} \times C_{eq} \Delta U_c^2$. After considering the percentage voltage fluctuations of capacitance $\pm\varepsilon$ $(0 \le \varepsilon \le 1)$ and the average total energy fluctuations in equivalent capacitance, the equivalent capacitance of MMC C_{eq} can be expressed as

$$C_{eq} = \frac{2P_s}{kw\varepsilon U_c^2} \left(1 - \left(\frac{k\cos\varphi}{2}\right)^2\right)^{\frac{3}{2}}. \quad (7)$$

Similar to a typical VSC–HVDC model, the steady-state external mathematical model of MMC–HVDC before the valve side shown in Fig. 2(b) under the dq frame can be obtained as

$$\begin{cases} L_i \dfrac{di_{sdi}}{dt} = -R_i i_{sdi} - wL_i i_{sqi} + U_{sdi} - U_{cdi} \\ L_i \dfrac{di_{sqi}}{dt} = -R_i i_{sdi} + wL_i i_{sqi} + U_{sqi} - U_{cqi} \\ C_{eq} \dfrac{dU_{dci}}{dt} = i_j - i_{dc} = \dfrac{3(\mathrm{U}_{cdi}\mathrm{i}_{sdi} + \mathrm{U}_{cqi}\mathrm{i}_{sqi})}{2U_{dci}} - i_{dci} \end{cases}. \quad (8)$$

III. Small-signal Model of Multi-terminal MMC–HVDC Considering the Generalized Control Strategy

A. Small-Signal Stability Model of MMC Connected to an Active AC Network

Considering the differences in the AC network and relevant control strategies, we study and propose matchable multi-terminal small-signal models. The PLL control strategy is used for an MMC converter connected to an active AC network, and the constant-frequency control strategy is commonly utilized for an MMC converter connected to a weak AC network or a passive network. Different expressions of the small-signal models are suggested to correspond to these two cases. A small-signal model of the DC network that includes a DC node and DC cable is theoretically built. At the end of this section, the authors suggest a generic form of the small-signal stability model suitable for multi-terminal MMC–HVDC.

1) State-Space Model of MMC Considering Dual Loop and 2nd Harmonic Circulating–Suppressing Controllers

A control block diagram of a dual-loop controller of MMC is shown in Fig. 3(a). The outer control strategy is used to control the active power or DC voltage and the reactive power, and it can provide the reference currents for the inner controller. Its dynamic equations can be obtained by

$$\begin{cases} i_{sdi}^* = (k_{pi1} + k_{ii1}/s)(P_i^* - P_i) \\ i_{sqi}^* = (k_{pi2} + k_{ii2}/s)(Q_i^* - Q_i) \end{cases}. \quad (9)$$

On the basis of Fig. 3(a), the MMC terminal voltage can be obtained from the inner current loop controller by decoupling the inner current, and the voltage equation can be expressed as

$$\begin{cases} U_{cdi(1)} = U_{sdi} - \omega L_i i_{sqi} - (k_{pi3} + k_{ii3}/s)(i_{sdi}^* - i_{sdi}) \\ U_{cqi(1)} = U_{sqi} + \omega L_i i_{sdi} - (k_{pi4} + k_{ii4}/s)(i_{sqi}^* - i_{sqi}) \end{cases}. \quad (10)$$

The typical circulating controller is often adopted in an MMC–HVDC system. According to Fig. 3(b), it satisfies

$$\begin{aligned} U_{cird(2)} &= (k_{cirp1} + k_{ciri1}/s)(i_{cird}^* - i_{cird}) + 2\omega L_0 i_{cirq} \\ &= k_{cirp1}(i_{cird}^* - i_{cird}) + 2\omega L_0 i_{cirq} + k_{ciri1} f_{i1} \\ U_{cirq(2)} &= (k_{cirp2} + k_{ciri2}/s)(i_{cirq}^* - i_{cirq}) - 2\omega L_0 i_{cird} \\ &= k_{cirp2}(i_{cirq}^* - i_{cirq}) - 2\omega L_0 i_{cird} + k_{ciri2} f_{i2} \end{aligned}. \quad (11)$$

In Eq. (11), $f_{i1} = \frac{1}{s}(i_{cird}^* - i_{cird})$ and $f_{i2} = \frac{1}{s}(i_{cirq}^* - i_{cirq})$. k_{cirp1}, k_{ciri1}, k_{cirp2}, and k_{ciri2} are the proportional and integral gains of the active and reactive power controllers.

For the multi-terminal HVDC system, a converter station must be operated as a balance node for the other stations. In Fig. 1, MMC2 is set as an equilibrium node because of its high short ratio. It uses constant DC voltage and a reactive power control strategy. Similar to Eq. (9), the outer control loop shown in Fig. 3(a) satisfies

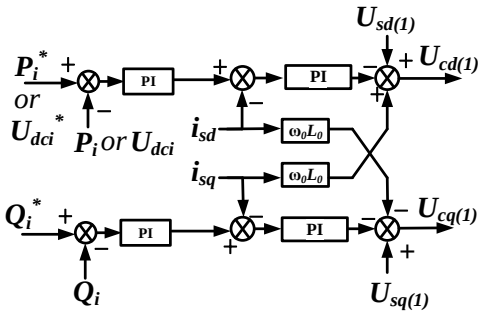

(a)

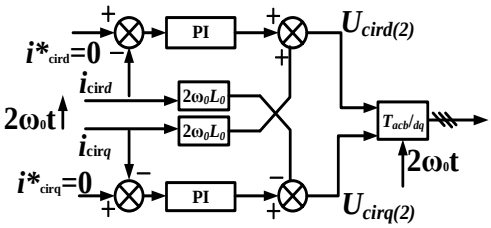

(b)

Fig. 3. Control block diagrams of dual-loop and circulating–suppressing controllers. (a) Dual-loop controller. (b) 2nd harmonic circulating–suppressing controller.

$$\begin{cases} i_{sdi}^* = (k_{pi1} + k_{ii1}/s)(U_{dci}^* - U_{dci}) \\ i_{sqi}^* = (k_{pi2} + k_{ii2}/s)(Q_i^* - Q_i) \end{cases}. \tag{12}$$

2) State-Space Model of PLL

PLL provides an angle reference for all other controllers, and the control accuracy of PLL is significantly affected by the short circuit ratio (SCR) of an AC network. The short circuit capacity of the AC system should be larger than the transmitted DC power to ensure the stable operation of MMC–HVDC [25]. A PLL control strategy is usually applied for an active AC network with a large SCR (larger than 1.24). The dynamic equation is

$$\theta_{PLL} = \int [(k_{\theta p} + k_{\theta i}/s)\sin(\theta_0 - \theta_{PLL}) + w_0]dt \,. \tag{13}$$

Given that all of the variables under the d-q frame are based on θ_{PLL},

$$U_{sq} = |U_s|\sin(\theta_{PLL} - \theta_0) \,. \tag{14}$$

Then, the small-signal state-space model of PLL can be expressed as

$$\frac{d\Delta\theta_{PLL}}{dt} = -k_{\theta p}\frac{\Delta U_{sq}}{|U_s|} - k_{\theta i}\Delta z_{pl} - jkw\Delta\theta_{PLL} \,, \tag{15}$$

where $\Delta U_{sq} = \Delta U_{sd}\sin\theta_0 + \Delta U_{sq}\cos\theta_0 + \Delta U_{sd}\Delta\theta_{PLL}$ and $\Delta z_{pl} = \int \Delta U_{sq}/|U_s|\,dt$.

To investigate the external characteristic of MMC–HVDC for power system stability analysis, the proposed small-signal model is represented as an equivalent AC–DC differential object that substitutes for the relative MMC–HVDC inner variable. The small-signal state-space model and its detailed derivation process are given in Appendix (A4).

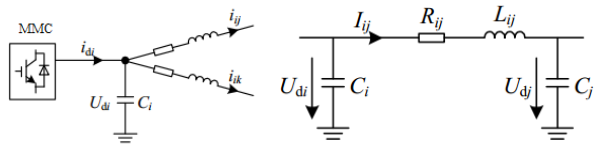

(a) (b)

Fig. 4. DC network model. (a) DC node model. (b) Equivalent model of DC line.

B. Small-Signal State-Space Model of MMC Connected to a Weak AC or Passive Network

In an AC power network whose SCR is relatively small, the constant-frequency control strategy is generally introduced for MMC–HVDC [26]. The dynamic equation can be obtained as

$$\begin{cases} i_{sdi}^* = (k_{pi5} + k_{ii5}/s)(U_{sdi}^* - U_{sdi}) \\ i_{sqi}^* = (k_{pi6} + k_{ii6}/s)(U_{sqi}^* - U_{sqi}) \\ \theta = 2\pi ft \end{cases}. \tag{16}$$

Usually, the voltage phase of the AC bus is selected as the reference ($U_{sd}^* = U_1^*$, $U_{sq}^* = 0$). Similarly, the small-signal state-space model can be expressed as (B1).

C. Small-Signal Model of the DC Network

The DC network of the MMC–HVDC system can be roughly divided into cyclic, radial, and reticular according to the network structure. Regardless of the applied structure, the MMC station can theoretically be regarded as a DC network model. A schematic of a typical DC network model that consists of DC nodes and DC lines is shown in Fig. 4.

The dynamic equation of a DC node derived by using Kirchhoff's law is

$$C_i\frac{dU_i}{dt} = i_i - \sum_{j=1}^{n} i_{dij} = \frac{3(U_{cdi}i_{sdi} + U_{cqi}i_{sqi})}{2U_{di}} - \sum_{j=1}^{n} i_{dij} \,. \tag{17a}$$

The linearized expression, which is indicated in the Appendix, is similar to Eq. (8). The small-signal model of the DC line's current equation should meet

$$L_{ij}\frac{d\Delta i_{dij}}{dt} = \Delta U_{di} - \Delta U_{dj} - R_{ij}\Delta i_{dij} \,. \tag{17b}$$

D. Generic Form of Small-signal Stability Model Suitable for Multi-terminal MMC–HVDC

On the basis of the aforementioned individual small-signal state-space models, a small-signal model of MMC–HVDC based on dynamic phasors can be deduced by

$$\frac{\mathbf{d\Delta x}}{\mathbf{dt}} = \mathbf{A\Delta x + B\Delta u} \,. \tag{18}$$

In terms of A(4) and B(1), $\boldsymbol{x}_k$ can be expressed as

$$\mathbf{\Delta x = [\Delta x_1, \Delta x_2, \Delta x_3, ..., |\Delta U_{di}|, |\Delta I_{di}|]} \,. \tag{19}$$

When an MMC station is connected to an active grid, then

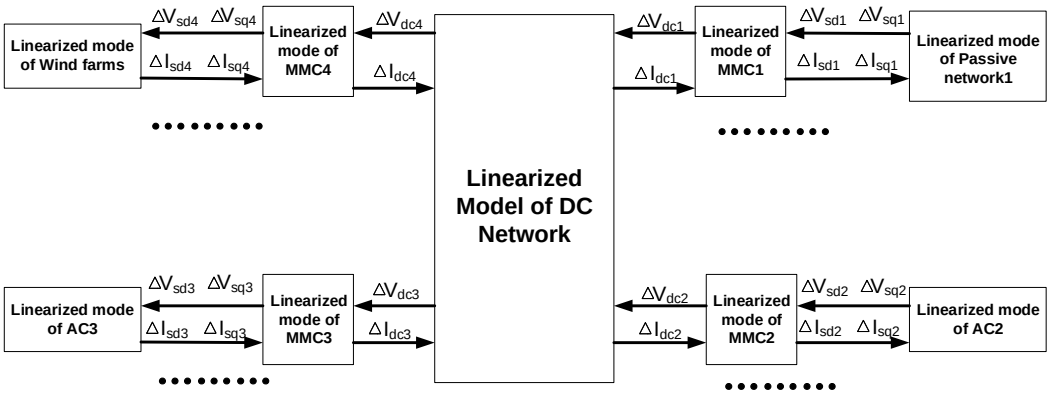

Fig. 5. Methodology used to obtain the complete small-signal model of a multi-terminal MMC–HVDC.

$$\mathbf{\Delta x_i}=[\Delta i_{sdi},\Delta i_{sqi},\Delta U_{sdi},\Delta U_{sqi},\Delta i_{cird},\Delta i_{cirq},\Delta z_{i1},\Delta z_{i2},\Delta z_{i3},\Delta z_{i4},\Delta f_1,\Delta f_2,\Delta\theta_{PLL},\Delta z_{pl}]^T \quad (20a)$$

When an MMC station is connected to a weak AC system or passive network, then

$$\mathbf{\Delta x_i}=[\Delta i_{sdi},\Delta i_{sqi},\Delta i_{cird},\Delta i_{cirq},\Delta z_{i5},\Delta z_{i6},\Delta z_{i7},\Delta z_{i8},\Delta f_1,\Delta f_2,\Delta\theta]^T \quad (20b)$$

$$\mathbf{\Delta U_{di}}=[\Delta U_{d1},\Delta U_{d2},\Delta U_{d3},.....]^T \quad (20c)$$

$\mathbf{\Delta I_{di}}$ is the current that flows through the DC network, and its expression can be obtained by (17b). $\mathbf{\Delta u_i}=[\Delta P_i,\Delta Q_i]^T$ or $\mathbf{\Delta u_i}=[\Delta U_{dci},\Delta Q_i]^T$ and $\mathbf{\Delta u_i}=[\Delta U_{sdi},\Delta U_{sqi}]^T$ are the respective active and weak AC control variable matrixes. DC current and DC voltage are applied to link the MMC station, and the other power elements, such as synchronous generators and wind farms, are connected to the MMC station by using Kirchhoff's law, as shown in Fig. 5. Consequently, a generic form of the small-signal state-space model of a multi-terminal MMC–HVDC is achieved.

IV. Advanced Small-signal Model based on the Dynamic Phasor Method

The mathematical basis of dyn.phasors is Fourier transform, and based on the generalized averaging theory, this method can represent the quasi-periodic switching nature of electronic devices by using time-varying Fourier coefficients. The computational simulation period can be reduced by selecting the dominant frequency of a system. $x(\tau)$ with cycle T is expressed with a Fourier series in any range $\tau\in(t-T,t]$ as

$$x(\tau)=\sum_{k=-\infty}^{\infty}X_k(t)e^{jkw\tau}, \quad (21)$$

where $w=2\pi/T$; $X_k(t)$ is the k-th harmonic Fourier coefficient, which is also called the k-th dynamic phasor.

$$X_k(t)=\frac{1}{T}\int_t^{t+T}x(\tau)e^{-jwt}d\tau=\langle x\rangle_k(t) \quad (22)$$

$X_k(t)$ is a time-varying function of a complex field, and it can be abbreviated as $\langle x\rangle_k$.

$$\langle x\rangle_k=\langle x\rangle_k^R+j\langle x\rangle_k^I=\langle x\rangle_{-k}^*=(\langle x\rangle_{-k}^R+j\langle x\rangle_{-k}^I)^*, \quad (23)$$

where subscripts R and I are the real and imaginary parts. $\langle x\rangle_k$ possesses the following properties.

1) Differential property

$$\frac{dX_k}{dt}=-jwX_k+\left\langle\frac{dx}{dt}\right\rangle_k \quad (24)$$

2) Convolution property

$$\langle x_1x_2\rangle_k=\sum_{i=-\infty}^{\infty}\langle x_1\rangle_{k-i}\langle x_2\rangle_i \quad (25)$$

For different components, including resistance, capacitance, and inductance, their dyn.phasor expressions are as follows:

$$\begin{cases}\langle u_R\rangle_k=R\langle i\rangle_k\\ \langle u_L\rangle_k=L\dfrac{d\langle i_L\rangle_k}{dt}+jkwL\langle i_L\rangle_k\\ \langle i_c\rangle_k=L\dfrac{d\langle u_c\rangle_k}{dt}+jkwC\langle u_c\rangle_k\end{cases}. \quad (26)$$

Accordingly, by utilizing Eqs. (25) and (26), the k-th linearized state-space model can be rewritten in terms of dyn.phasors as

$$\frac{d\langle\mathbf{\Delta x}\rangle_k}{dt}=A\langle\mathbf{\Delta x}\rangle_k+B\langle\mathbf{\Delta u}\rangle_k-jkw\langle\mathbf{\Delta x}\rangle_k, \quad (27)$$

where the property of dyn.phasors (24)–(26) is used to build Eq. (27). The small-signal model under the formatting of dyn.phasors can be identified based on Eq. (27). In the case of retaining main-order phasors and selecting appropriate Fourier coefficients, this dynamic method can efficiently simplify the EMT simulation procedure and satisfy variable precision [27].

Built on an innovative idea, this work establishes the small-signal model of multi-terminal MMC–HVDC based on dyn.phasors through the following steps.

1) Establishing traditional stability models in consideration of different control strategies.

2) Calculating each harmonic component and rewriting the related contents in terms of dyn.phasors.
3) Merging each dynamic phasor into the fundamental component and building the advanced small-signal model.

The next step is to select an appropriate harmonic component that addresses concerns on accuracy and computational burden. We assume that the fundamental frequency is f_0 and $\omega = 2\pi f_0$, the Fourier series is the basis of the frequency component. According to Eqs. (4) and (5), the Fourier series of the AC side current should include the ±1st and ±2nd-order dynamic phasors, and the Fourier series of the DC voltage should include the ±1st-, ±2nd-, and ±3rd-order dynamic phasors and DC component.

Considering the negative sequence, the DC voltage and AC side current of MMC–HVDC can be written as follows:

$$\begin{aligned} i_j(t) &= \langle i_j \rangle_1 e^{j\omega t} + \langle i_j \rangle_{-1} e^{-j\omega t} + \langle i_j \rangle_2 e^{j2\omega t} + \langle i_j \rangle_{-2} e^{-j2\omega t} \\ &= 2\mathrm{Re}\left(\langle i_j \rangle_1 e^{j\omega t} + \langle i_j \rangle_2 e^{j2\omega t} \right) \end{aligned} , \quad (28a)$$

$$\begin{aligned} u_d(t) &= u_{dc} + \langle u_d \rangle_1 e^{j\omega t} + \langle u_d \rangle_{-1} e^{-j\omega t} + \langle u_d \rangle_2 e^{j2\omega t} \\ &\quad + \langle u_d \rangle_{-2} e^{-j2\omega t} + \langle u_d \rangle_3 e^{j3\omega t} + \langle u_d \rangle_{-3} e^{j3\omega t} \\ &= u_{dc} + 2\mathrm{Re}\left(\langle u_d \rangle_1 e^{j\omega t} + \langle u_d \rangle_2 e^{j2\omega t} + \langle u_d \rangle_3 e^{j3\omega t} \right) \end{aligned} . \quad (28b)$$

Calculations for the current–voltage dynamic phasors are carried out based on the three steps, and Eq. (27) is introduced for merging each phasor into the fundamental component. Although the system eigenvalues might be shifted on the imaginary axis ($-jk\omega$) by utilizing a dynamic phasor, by introducing Eq. (28), the proposed model can compensate for this shift and be reasonable for power system analysis. The following calculations are for the current–voltage dynamic phasor components.

The first AC current can be obtained by the linearized form in A1. According to the KVL theorem and Eq. (1), the second circulating current under the dq0 frame meets

$$\begin{cases} L_0 \dfrac{di_{2d}}{dt} = 2\omega_0 i_{2q} - R_0 i_{2d} + \dfrac{1}{2}(U_{j,p} + U_{j,n} - U_{DC})_{d2} \\ L_0 \dfrac{di_{2q}}{dt} = -2\omega_0 i_{2d} - R_0 i_{2q} + \dfrac{1}{2}(U_{j,p} + U_{j,n} - U_{DC})_{q2} \end{cases} , \quad (29)$$

where i_{2d} and i_{2q} are the second circulating currents under the dq0 frame. We assume that the voltage per SM is equal and constant. Then, the voltage in the arm can be obtained by

$$\begin{aligned} U_{j,p} &= u_{j,p}^{sum} \bullet S_p = S_p \bullet N \bullet u_{cp} \\ U_{j,n} &= u_{j,n}^{sum} \bullet S_n = S_n \bullet N \bullet u_{cn} \end{aligned} . \quad (30)$$

The SM capacitor voltage, u_c, (i.e., u_{cp} or u_{cq}) meets Eq. (5). Substituting Eqs. (2) and (30) into Eq. (29) while neglecting the 3rd and 4th harmonics yields the equation

$$\begin{cases} L_0 \dfrac{di_{2d}}{dt} = 2\omega_0 i_{2q} - R_0 i_{2d} + \dfrac{N}{4}(-M_{1d} u_{c1d} + M_{1q} u_{c1q} + 2u_{c2d} - 2M_{2d} u_{dc}) \\ L_0 \dfrac{di_{2q}}{dt} = -2\omega_0 i_{2d} - R_0 i_{2q} + \dfrac{N}{4}(-M_{1q} u_{c1q} - M_{1d} u_{c1d} + 2u_{c2q} - 2M_{2q} u_{dc}) \end{cases} . \quad (31)$$

To obtain the ±1st-, ±2nd-, and ±3rd-order voltage phasor components, the injected current equations flowing through the capacitor are utilized.

$$S_p \frac{du_{j,p}^{sum}}{dt} + S_n \frac{du_{j,n}^{sum}}{dt} = \frac{du_d}{dt} \quad (32)$$

Combined with Eq. (1), Eq. (32) can be rewritten as

$$\frac{du_d}{dt} = -\frac{1}{C_0}\left[(S_p^2 + S_n^2) \cdot i_{cir} - \frac{S_p^2 - S_n^2}{2} i_{sj} \right] . \quad (33)$$

If the circulating current has no basic frequency component, then

$$i_{cir} = \frac{i_{dc}}{3} + i_2 \cos(2\omega t + \varphi_2) . \quad (34)$$

We manipulate Eqs. (2), (32), and (34) into Eq. (33), transfer them to the dq0 frame, and merge the similar terms accordingly (ignoring the high-frequency component). Thus, the DC voltage phasor dynamic is obtained.

$$\begin{cases} \dfrac{du_{1d}}{dt} = \dfrac{1}{C_0}[-(\dfrac{1}{4}M_{1q}M_{2q} - \dfrac{1}{2}M_{1q})i_{sd} + (\dfrac{1}{4}M_{1d}M_{2d} - \dfrac{1}{2}M_{1d})i_{sq} \\ \qquad - \omega u_{1q} - \dfrac{1}{6} i_{dc} M_{1d}] \\ \dfrac{du_{1q}}{dt} = \dfrac{1}{C_0}[-(\dfrac{1}{4}M_{1d}M_{2d} - \dfrac{1}{2}M_{1d})i_{sq} + (\dfrac{1}{4}M_{1q}M_{2q} - \dfrac{1}{2}M_{1q})i_{sd} \\ \qquad + \omega u_{1d} - \dfrac{1}{6} i_{dc} M_{1q}] \end{cases} \quad (35)$$

$$\begin{cases} \dfrac{du_{2d}}{dt} = \dfrac{1}{C_0}[-\omega u_{2q} - \dfrac{1}{6} i_{dc}(\dfrac{1}{2}M_{1d}^2 - 2M_{2d}) - \dfrac{1}{2} i_{2d} M_{1d} - \\ \qquad \dfrac{1}{4}(\dfrac{1}{2}M_{1d}M_{2d} - M_{1d})i_{sd} + \dfrac{1}{4}(\dfrac{1}{2}M_{1d}M_{2d} - M_{1d})i_{sq}] \\ \dfrac{du_{2q}}{dt} = \dfrac{1}{C_0}[\omega u_{2d} - \dfrac{1}{6} i_{dc}(\dfrac{1}{2}M_{1q}^2 - 2M_{2q}) - \dfrac{1}{2} i_{2q} M_{1q} - \\ \qquad \dfrac{1}{4}(\dfrac{1}{2}M_{1q}M_{2q} - M_{1q})i_{sq} + \dfrac{1}{4}(\dfrac{1}{2}M_{1q}M_{2q} - M_{1q})i_{sd}] \end{cases} \quad (36)$$

$$\begin{cases} \dfrac{du_{3d}}{dt} = \dfrac{1}{C_0}[-\omega u_{3q} - \dfrac{1}{2}M_{1d} i_{2d} + \dfrac{1}{2}M_{1q} i_{2q} - \dfrac{1}{2}M_{1d}M_{2d} i_{sd} \\ \qquad + \dfrac{1}{2}M_{1d}M_{2d} i_{sq}] \\ \dfrac{du_{3q}}{dt} = \dfrac{1}{C_0}[\omega u_{3d} - \dfrac{1}{2}M_{1q} i_{2q} + \dfrac{1}{2}M_{1d} i_{2d} - \dfrac{1}{2}M_{1q}M_{2q} i_{sq} \\ \qquad + \dfrac{1}{2}M_{1q}M_{2q} i_{sd}] \end{cases} \quad (37)$$

The linearized forms of the fundamental voltage component are expressed as Eqs. (A4) and (B1). The dyn.phasor expressions of Eqs. (31) and (35)–(37) can be obtained by using Eqs. (25) and (26). The dyn.phasor expression of each component is not provided due to space limitations in this paper. Furthermore, by transferring the obtained components from the dq0 to the abc frame and by utilizing Eq. (28), the dynamic phasors are merged into the fundamental component. According to the aforementioned steps, the advanced small-signal model of the multi-terminal MMC–HVDC based

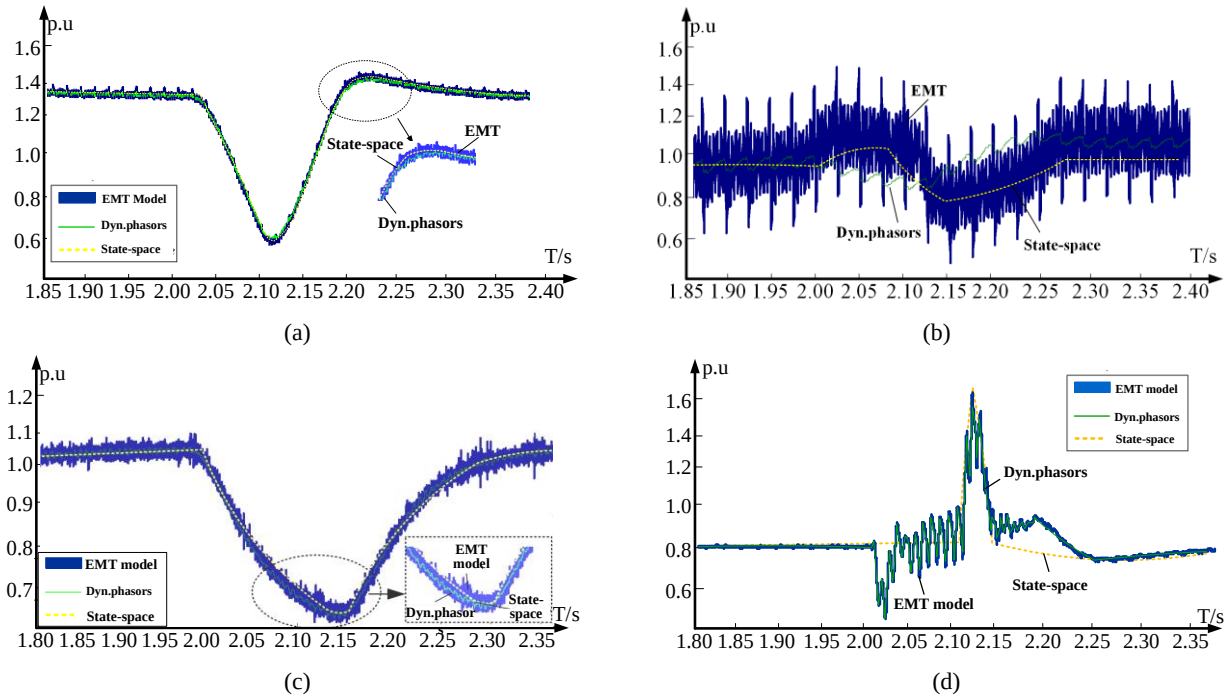

Fig. 6. Response of the MMC1 converter. (a) D-axis AC current. (b) Q-axis AC current. (c) Direct voltage. (d) Direct current.

on dynamic phasors is achieved, and it can be fulfilled under MATLAB/Simulink.

V. Model Analysis and Verification

A. Case Background

To estimate the validity and applicability of the proposed method, we establish a typical ±320 kV bipolar multi-terminal MMC–HVDC system via MATLAB/Simulink. The power capacity of each MMC converter, the PI control parameters, and the DC link inductor are indicated in Fig. 1. The results are compared with those of traditional state-space and EMT models that are built in Matlab/Simulink and EMTDC, respectively. The detailed simulation parameters are shown in Table I. The linearized operation point is selected for consistency with the power flow results in Fig. 1.

The dynamic small-signal model of DFIGs in [28] is introduced. In light of the "small" disturbance whose fluctuation margin is 10%–20% occurring in the MMC–HVDC network [29], related simulation analyses under different cases are performed to assess performance.

Case 1: Step change from 1.0 p.u. to 0.8 p.u. (change time: 2 s) in active power of MMC4.

Case 2: Reduction in active power (10%) and reactive power (5%) of MMC3 (change time: 2 s).

B. Performance Assessment of Case 1

The dynamic response of the multi-terminal HVDC network under case 1 is shown in Figs. 6 to 9. Although the traditional small-signal state-space model settles into the correct steady-state value of the actual response, it fails to show the transient oscillation of the multi-terminal MMC–HVDC network and has considerable errors during the transient period. The reason for this deviation is that the traditional model, based on the quasi-steady state assumption, considers only the basic frequency impedance. By contrast, the advanced small-signal model considers more high-frequency dynamic characteristics of electronic devices. As shown in Figs. 6 to 9, this advanced model can successfully follow the EMT response with small transient errors and can predict the damped oscillations at a certain moment.

Notably, the traditional and advanced state-space models present several errors, although they converge to a steady-state value. The reason for the errors is that the advanced model is developed by adopting only main frequency orders. By introducing more orders, the advanced model can obtain high calculation accuracy. In addition, the precision of the EMT model depends on small-step calculation, and the calculation process is highly complicated.

TABLE I
MMC Converter Parameters

Smoothing inductance	50 mH
Number of equivalent SMs	400
Capacitance per SM	10 mF
Sum of capacitor voltages at time zero	0 kV
Capacitor leakage resistance	10 MΩ
IGBT on resistance	0.001 Ω
IGBT off resistance	100 MΩ
Diode on resistance	0.001 Ω
Diode off resistance	100 MΩ

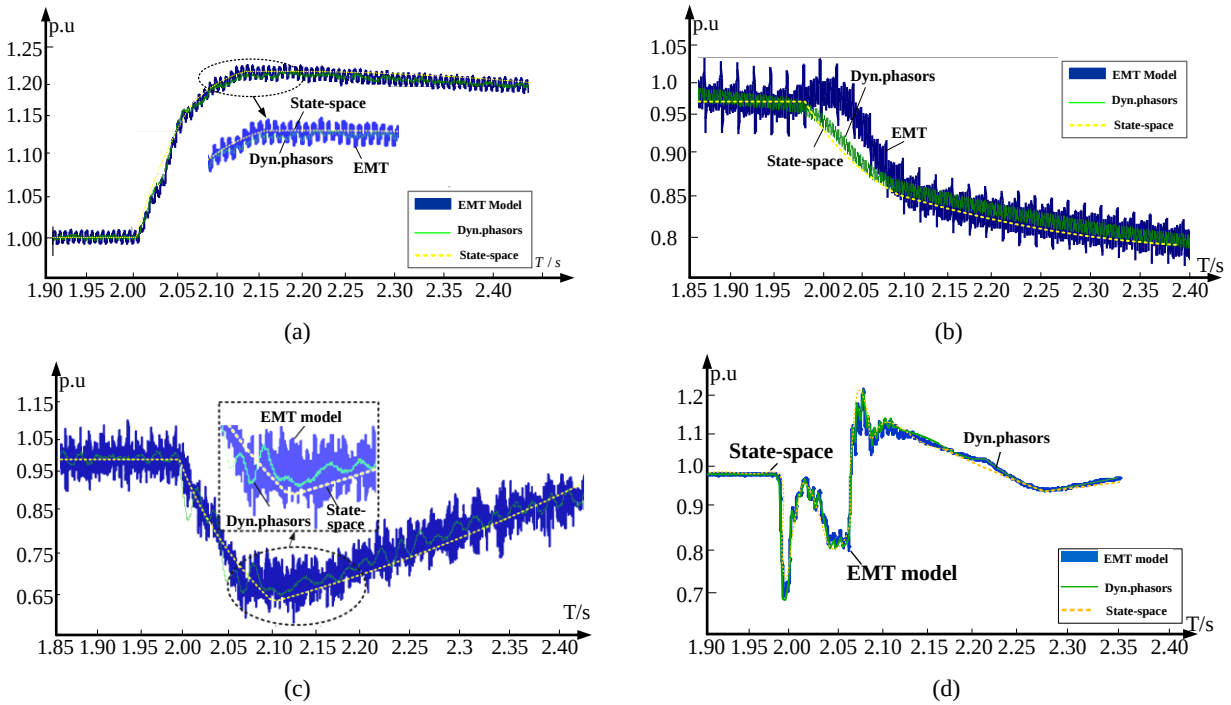

Fig. 7. Response of the MMC2 converter. (a) D-axis AC current. (b) Q-axis AC current. (c) Direct voltage. (d) Direct current.

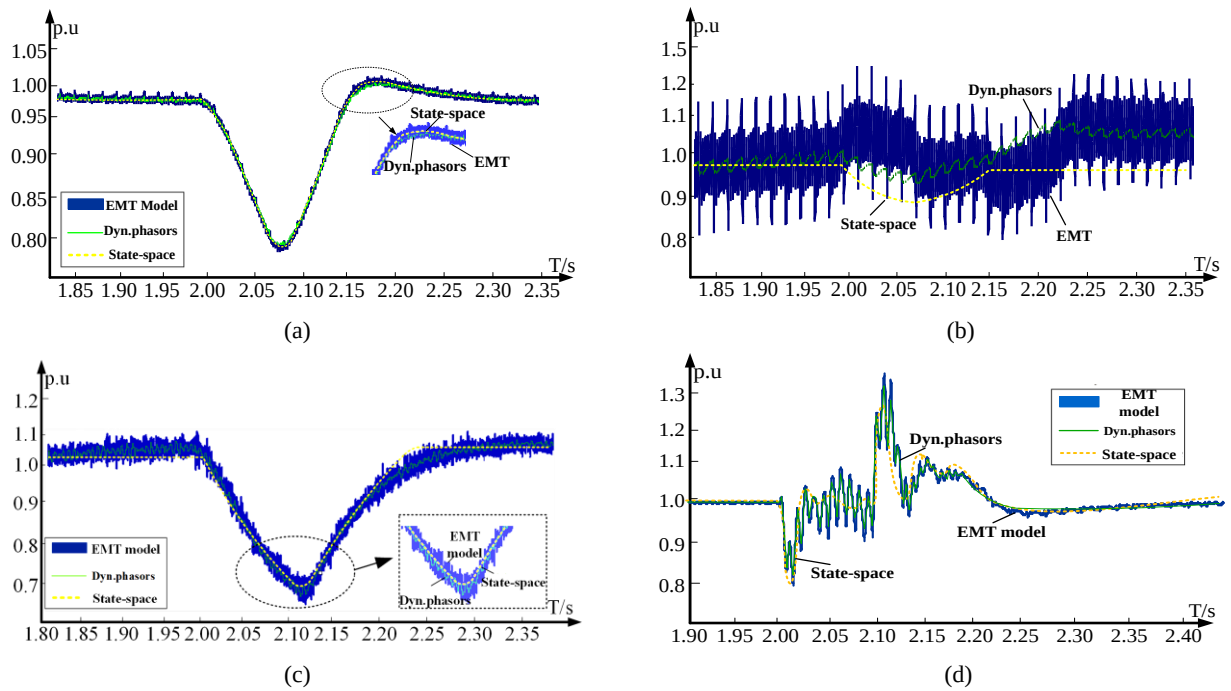

Fig. 8. Response of the MMC3 converter. (a) D-axis AC current. (b) Q-axis AC current. (c) Direct voltage. (d) Direct current.

The dyn.phasor model exerts a time-lead effect on the system response when disturbance occurs. This effect may cause errors, which may become highly obvious in the initial and end stages of the disturbance. In theory, this time-lead effect originates from a transfer process when introducing Eq. (28) for the merging component; that is, $e^{j\omega t}$ and $e^{j2\omega t}$ may exert a time-lead effect on the dynamic behavior of the model. The networks connected with MMC1 or MMC4 are weak AC systems, in which constant AC voltage is often introduced. In this situation, a common treatment method is to let $U_{ac} \approx U_d$, which ignores the q-axis response and causes possible errors. The wind farm connected to MMC4 is theoretically regarded as an oscillation source and may increase errors in the q-axis response, and AC network 1 is unable to resist the fluctuation because of its weak short ratio. In most cases, researchers wish to determine the stability

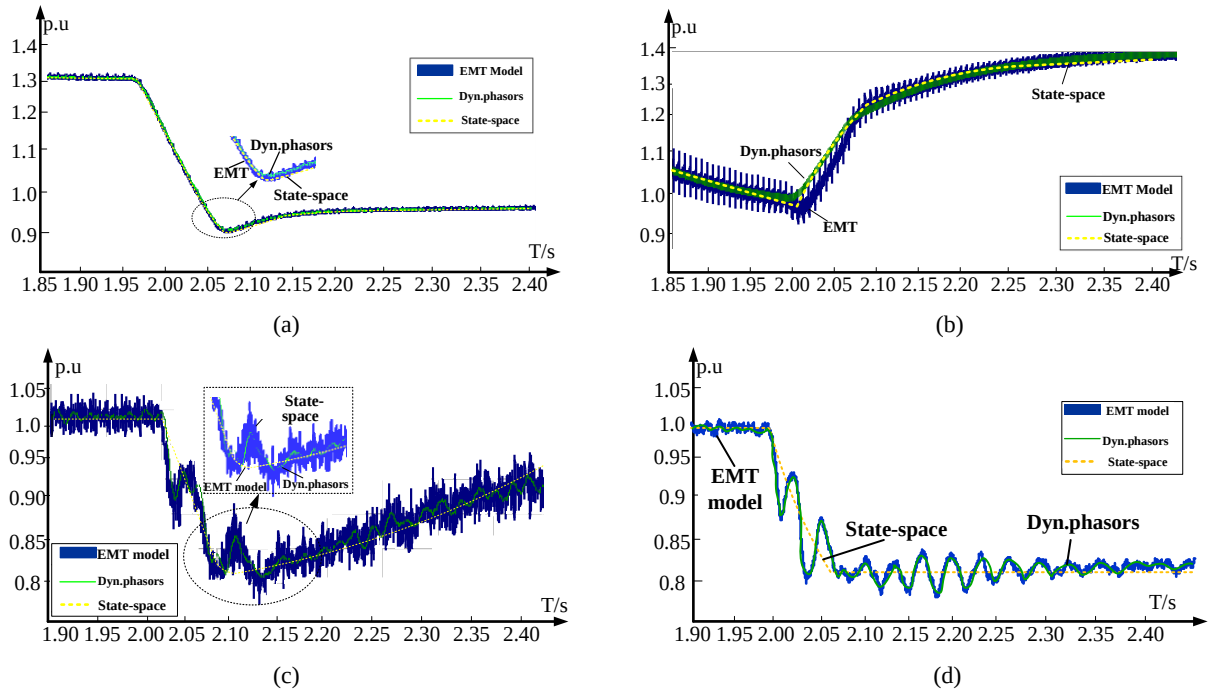

Fig. 9. Response of the MMC4 converter. (a) D-axis AC current. (b) Q-axis AC current. (c) Direct voltage. (d) Direct current.

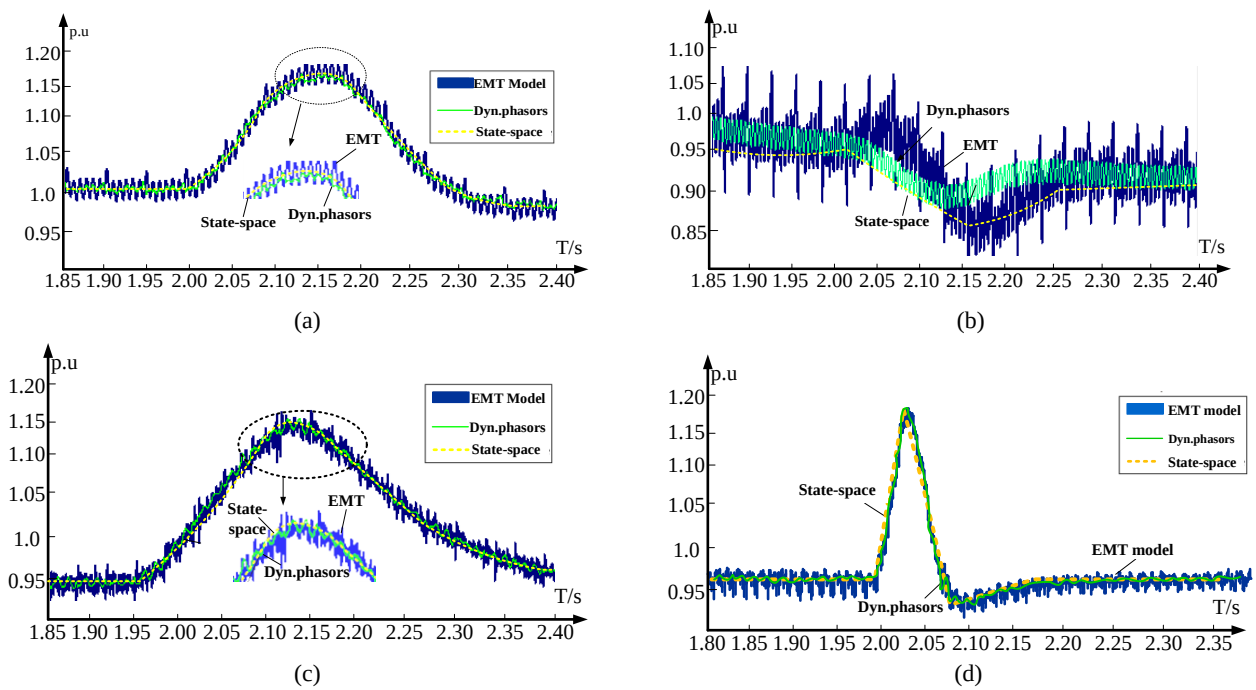

Fig. 10. Response of the MMC1 converter. (a) D-axis AC current. (b) Q-axis AC current. (c) Direct voltage. (d) Direct current.

margin and eigenvalue of a system. The dyn.phasor-based model is sufficiently accurate to identify system-dominant electromechanical oscillation modes.

C. Performance Assessment of Case 2

The dynamic response of the multi-terminal HVDC network under case 2 is shown in Figs. 10 to 13. The advanced model is able to follow the system response, including a sharp rise in current and voltage. Owing to the increase in calculation accuracy, this advanced model can be successfully utilized to analyze the dynamic performance of hybrid AC–DC systems. Improved understanding of AC system representation can thus be obtained.

In Fig. 13(b), the frequency of the fluctuation in the dyn.phasor model does not coincide with that in the EMT model. As mentioned previously, a wind farm connected to MMC4 is often regarded as an oscillation source, and the dyn.phasor model does not consider its power fluctuation and

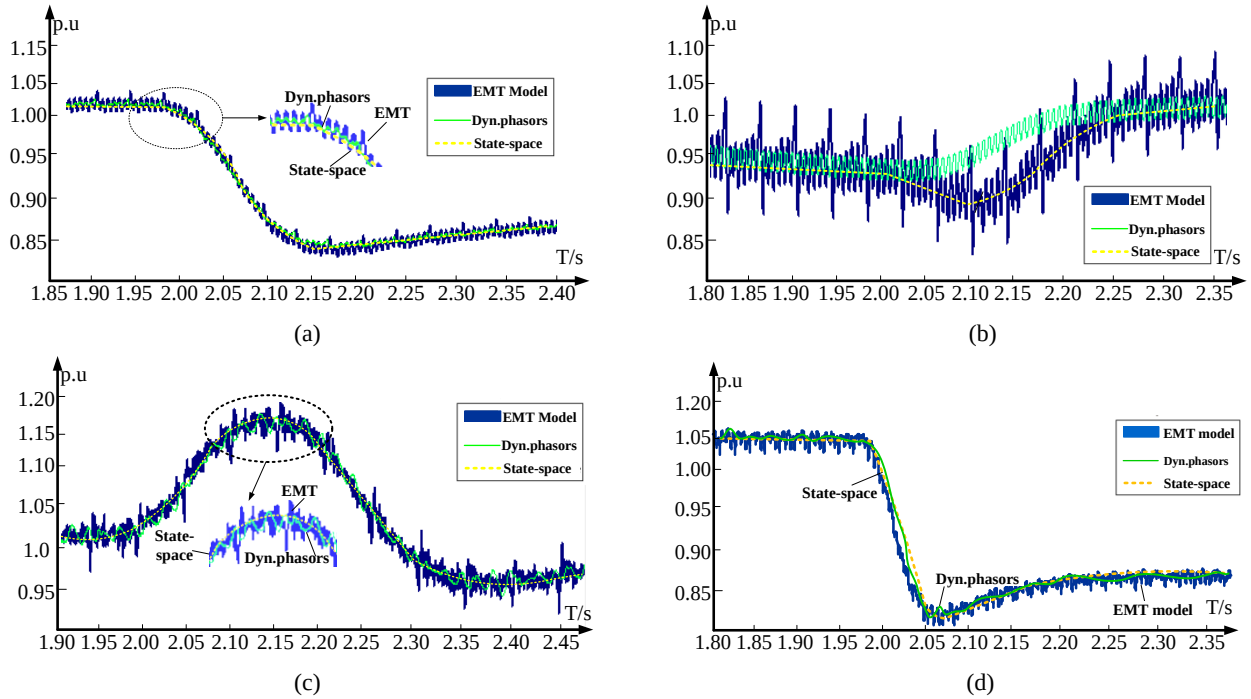

Fig. 11. Response of the MMC2 converter. (a) D-axis AC current. (b) Q-axis AC current. (c) Direct voltage. (d) Direct current.

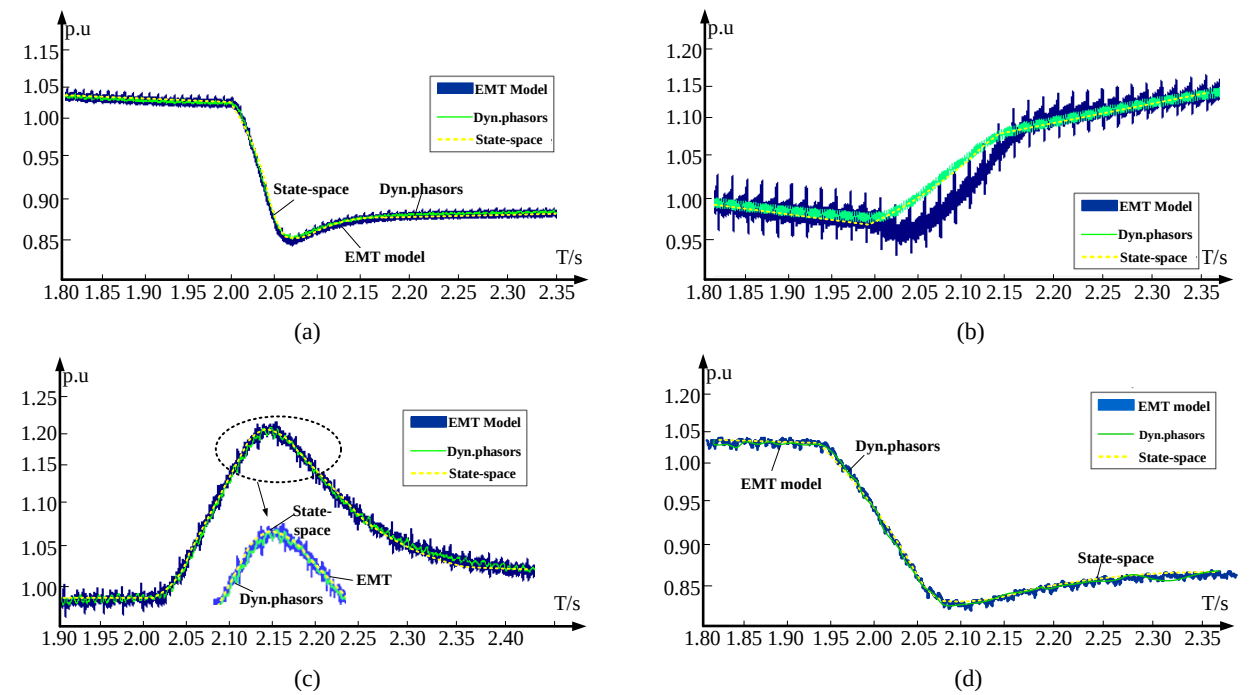

Fig. 12. Response of the MMC3 converter. (a) D-axis AC current. (b) Q-axis AC current. (c) Direct voltage. (d) Direct current.

harmonics during simulation. By contrast, in Case 2 [reduction in active power (10%) and reactive power (5%) of MMC3], the dyn.phasor model does not consider the effect of other converter stations when disturbances occur. Therefore, the dyn.phasor-based model still needs to be improved and should consider the impact of uncertainty and interaction between MMC and HVDC. These issues will be considered in the future.

Fig. 14 is added to show a comparison of the three models in the same frequency range and to further verify the frequency response of the proposed method. The frequency response of state-space and dyn.phasor models against that of the EMT model in the same frequency range is shown in Fig. 14. The dyn.phasor model exhibits acceptable matching, especially in the frequency range exceeding 50 Hz.

Investigating the benefits of the advanced model in

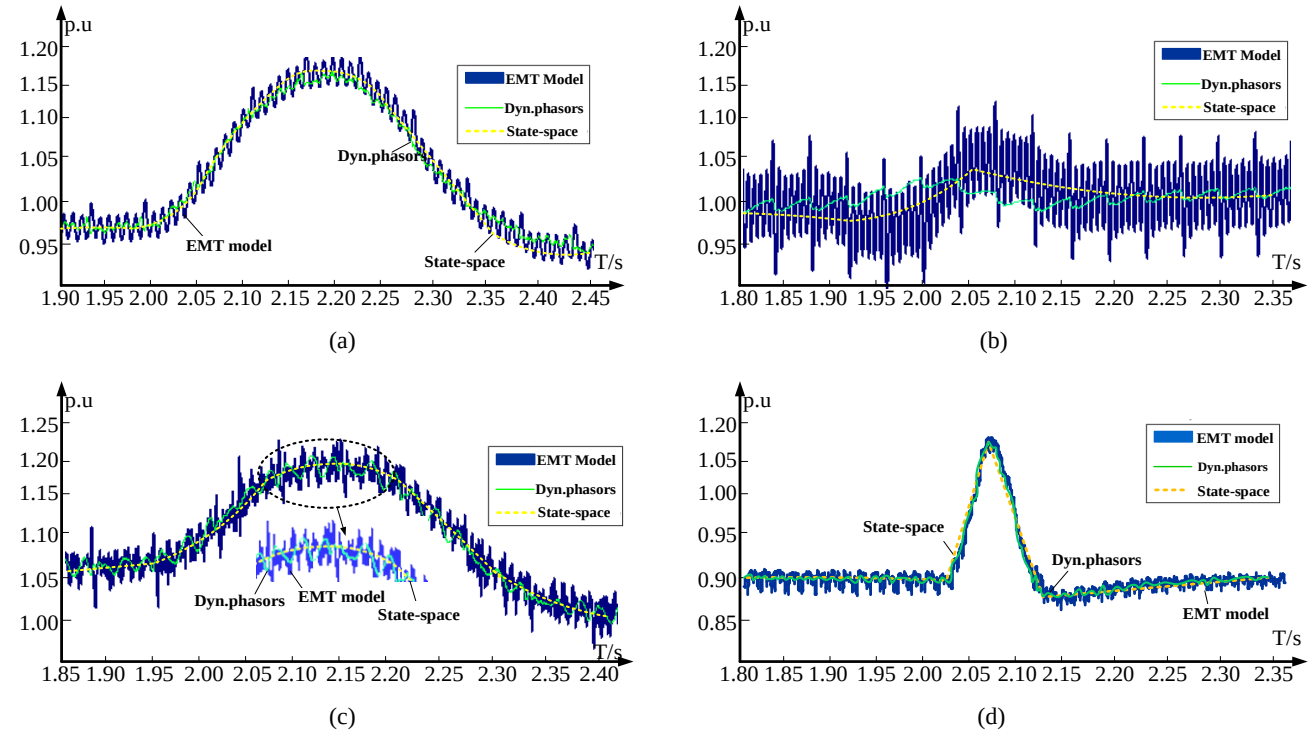

Fig. 13. Response of the MMC4 converter. (a) D-axis AC current. (b) Q-axis AC current. (c) Direct voltage. (d) Direct current.

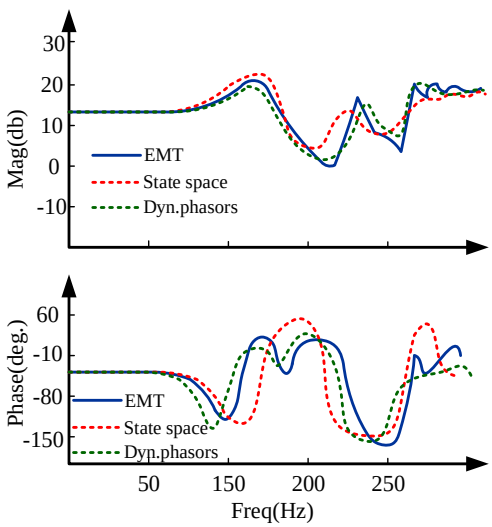

Fig. 14. Frequency response for state-space and dyn.phasor models.

TABLE II
RUNNING TIME OF SIMULATION UNDER THE THREE MODELS

	Advanced model	Traditional state-space model	Time-domain model
Case 1	24.97 s	3.82 s	421.723 s
Case 2	24.21 s	3.38 s	397.549 s

Note: The simulation time length is 0 s to 4 s.

accelerating simulation time is also important. The models in Matlab/Simulink are solved by fifth-order Runge-Kutta with 1 ms time steps, whereas the EMT model in PSCAD adopts its default method with 50 μs time steps. The running time of the test system under the three models is presented, and the comparison results are shown in Table II. During the simulation, calculation is carried out using a personal laptop (Intel Pentium (R) G630 with 2.70 GHz CPU and 4 GB of RAM).

Given that high-frequency components are disregarded in the advanced model, this model can use a large time step to speed up the simulation. Although the traditional state-space model possesses the smallest simulation time among the three models, its calculation accuracy should be improved further. In consideration of the two technical indicators, the advanced small-signal state-space model is a promising option.

VI. CONCLUSION

We propose an advanced small-signal stability model for multi-terminal MMC–HVDC to enhance the computational accuracy of stability analysis and reduce the simulation time. This model is compared with two conventional models. A related theoretical analysis and a simulation study are performed, and the results demonstrate the following:

1) To expand the application of the proposed advanced model for multi-terminal MMC–HVDC, this work establishes a linearized model that contains high harmonics and dynamics of internal variables in accordance with active and passive network control strategies.
2) Compared with the time-domain simulation model and

traditional small-signal state-space model, the advanced small-signal model can effectively decrease the errors of the quasi-steady state assumption and reduce the simulation time, and it can be efficiently utilized in the modeling of electronic devices.

3) The advanced small-signal stability model maintains low-frequency components, and it can successfully follow the EMT response and effectively predict the damped oscillations at a certain moment. However, the accuracy of this advanced model can still be improved by applying high-order phasors. Creating balance between computation burden and accuracy in the future is an issue that should be studied.

With regard to the proposed small-signal state-space model, a few aspects should be enriched, and these include optimizing and designing operation parameters of multi-terminal MMC–HVDC. Moreover, investigating the small-signal stability of large-scale hybrid AC–DC systems is necessary. These related topics will be tested with small-power experimental prototypes of MMC systems to improve the quality of future research. These tasks will be carried out in the future.

APPENDIX

A. Traditional Small-signal Analysis Model for Active Networks

To obtain the generic form of the model in an AC network, linearized Eqs. (9) and (10) can be expressed as

$$\begin{cases}\Delta i_{sdi}^{*}=-k_{pi1}\Delta P_i+k_{ii1}\Delta z_{i1}\\ \Delta i_{sqi}^{*}=-k_{pi2}\Delta Q_i+k_{ii2}\Delta z_{i2}\end{cases}, \tag{A1}$$

$$\begin{cases}\Delta U_{cdi(1)}=\Delta U_{sdi}-wL_i\Delta i_{sqi}-k_{pi3}(\Delta i_{sdi}^{*}-\Delta i_{sdi})-k_{ii3}\Delta z_{i3}\\ \Delta U_{cqi(1)}=\Delta U_{sqi}+wL_i\Delta i_{sdi}-k_{pi4}(\Delta i_{sqi}^{*}-\Delta i_{sqi})-k_{ii4}\Delta z_{i4}\end{cases}. \tag{A2}$$

We let $z_{i1}=\int(P_i^{*}-P_i)$ $z_{i2}=\int(Q_i^{*}-Q_i)$, $z_{i3}=\int(i_{sdi}^{*}-i_{sdi})$, and $z_{i4}=\int(i_{sqi}^{*}-i_{sqi})$. Moreover, $z_{i1}=\int(U_{dci}^{*}-U_{dci})$ and $z_{i2}=\int(Q_i^{*}-Q_i)$ when DC voltage control is introduced.

Given that $i_{cird}^{*}=0$ and $i_{cirq}^{*}=0$, the linearized forms of Eq. (11) are

$$\begin{cases}\Delta U_{cird(2)}=-k_{cirp1}\Delta i_{cird}+2\omega L_0\Delta i_{cirq}+k_{ciri1}\Delta f_1\\ \Delta U_{cirq(2)}=-k_{cirp2}\Delta i_{cirq}-2\omega L_0\Delta i_{cird}+k_{ciri2}\Delta f_2\end{cases}. \tag{A3}$$

By manipulating (A1) into (A2) and merging with (A3) accordingly, voltage components ΔU_{cdi} and ΔU_{cqi} can be obtained. Then, by using these voltage components to substitute for the corresponding terms in the linearized form of Eq. (8), the generalized small-signal MMC–HVDC model can be indicated as A4.

$$\begin{aligned}L_i\frac{d\Delta i_{sdi}}{dt}=&-(R_i+k_{pi3})\Delta i_{sdi}-k_{pi3}k_{pi1}\Delta P_i+k_{pi3}k_{ii1}\Delta z_{i1}+k_{ii3}\Delta z_{i3}\\&+k_{cirp1}\Delta i_{cird}-2\omega L_0\Delta i_{cirq}-k_{ciri1}\Delta f_1\end{aligned}, \tag{A4a}$$

$$\begin{aligned}L_i\frac{d\Delta i_{sqi}}{dt}=&-(R_i+k_{pi4})\Delta i_{sqi}-k_{pi4}k_{pi2}\Delta Q_i+k_{pi4}k_{ii2}\Delta z_{i2}+k_{ii4}\Delta z_{i4}\\&+k_{cirp2}\Delta i_{cirq}+2\omega L_0\Delta i_{cird}-k_{ciri2}\Delta f_2\end{aligned}, \tag{A4b}$$

$$\begin{aligned}C_{eq}\frac{d\Delta U_{dci}}{dt}=&-\frac{3k_{ii4}i_{sqi}}{2U_{dci}}\Delta z_{i4}+\frac{3k_{ciri1}i_{sdi}}{2U_{dci}}\Delta f_1+\frac{3k_{ciri2}i_{sqi}}{2U_{dci}}\Delta f_2\\&-[\frac{3(U_{cdi}i_{sdi}+U_{cqi}i_{sqi})}{2U_{dci}^{2}}]\Delta U_{dci}+\frac{3k_{pi3}k_{pi1}i_{sdi}}{2U_{dci}}\Delta P_i\\&-\frac{3\Delta i_{cird}}{2U_{dci}}(k_{cirp1}i_{sdi}+2\omega_0L_0i_{sqi})+\frac{3k_{pi2}k_{pi4}i_{sqi}}{2U_{dci}}\Delta Q_i\\&-\frac{3\Delta i_{cirq}}{2U_{dci}}(k_{cirp2}i_{sqi}-2\omega_0L_0i_{sdi})-\frac{3k_{ii1}k_{pi1}i_{sdi}}{2U_{dci}}\Delta z_{i1}\\&+\frac{3}{2U_{dci}}\left[i_{sdi}\Delta U_{sdi}+i_{sqi}\Delta U_{sqi}\right]-\frac{3k_{ii2}k_{pi2}i_{sqi}}{2U_{dci}}\Delta z_{i2}\\&+\frac{3\Delta i_{sdi}}{2U_{dci}}(U_{cdi}+\omega L_ii_{sqi}+k_{pi3}i_{sdi})-\frac{3k_{ii3}i_{sdi}}{2U_{dci}}\Delta z_{i3}\\&+\frac{3\Delta i_{sqi}}{2U_{dci}}(U_{cqi}-\omega L_ii_{sdi}+k_{pi4}i_{sqi})-\Delta i_{dci}\end{aligned}, \tag{A4c}$$

where ΔP_i and ΔQ_i can be attained by the following equation.

$$\begin{aligned}\Delta P_i&=1.5[i_{sd}\Delta U_{sd}+U_{sd}\Delta i_{sd}+i_{sq}\Delta U_{sq}+U_{sq}\Delta i_{sq}]\\ \Delta Q_i&=1.5[i_{sq}\Delta U_{sd}+U_{sd}\Delta i_{sq}-i_{sd}\Delta U_{sq}-U_{sq}\Delta i_{sd}]\end{aligned} \tag{A4d}$$

When the DC bus control strategy is used, the small-signal model under this situation can be obtained by substituting ΔU_{dci} for ΔP_i. Owing to page length limitations, the detailed formation is not provided here.

B. Traditional Small-signal Analysis Model for Passive Network

The pattern of a passive network model of MMC–HVDC is similar to (A4). Combined with Eq. (15), the small-signal state-space model can be expressed as

$$\begin{aligned}L_i\frac{d\Delta i_{sdi}}{dt}=&-(R_i+k_{pi7})\Delta i_{sdi}-k_{pi7}k_{pi5}\Delta U_{sdi}+k_{pi7}k_{ii5}\Delta z_{i5}+k_{ii7}\Delta z_{i6}\\&+k_{cirp1}\Delta i_{cird}-2\omega L_0\Delta i_{cirq}-k_{ciri1}\Delta f_1\end{aligned}, \tag{B1a}$$

$$\begin{aligned}L_i\frac{d\Delta i_{sqi}}{dt}=&-(R_i+k_{pi8})\Delta i_{sqi}-k_{pi6}k_{pi8}\Delta U_{sqi}+k_{pi8}k_{ii6}\Delta z_{i6}+k_{ii8}\Delta z_{i8}\\&+k_{cirp2}\Delta i_{cirq}+2\omega L_0\Delta i_{cird}-k_{ciri2}\Delta f_2\end{aligned}, \tag{B1b}$$

$$\begin{aligned}C_{eq}\frac{d\Delta U_{dci}}{dt}=&\frac{3i_{sdi}}{2U_{di}}(1+k_{pi7}k_{pi5})\Delta U_{sdi}-\frac{3k_{ii5}k_{pi5}i_{sdi}}{2U_{dci}}\Delta z_{i5}\\&+\frac{3i_{sqi}}{2U_{dci}}(1+k_{pi6}k_{pi8})\Delta U_{sqi}-\frac{3k_{ii6}k_{pi6}i_{sqi}}{2U_{dci}}\Delta z_{i6}\\&+\frac{3}{2U_{di}}(U_{cdi}+wL_ii_{sqi}+k_{pi7}i_{sdi})\Delta i_{sdi}-\frac{3k_{ii7}i_{sdi}}{2U_{dci}}\Delta z_{i7}\\&-\frac{3\Delta i_{cird}}{2U_{dci}}(k_{cirp1}i_{sdi}+2\omega_0L_0i_{sqi})+\frac{3k_{ciri1}i_{sdi}}{2U_{dci}}\Delta f_1\\&-\frac{3\Delta i_{cirq}}{2U_{dci}}(k_{cirp2}i_{sqi}-2\omega_0L_0i_{sdi})+\frac{3k_{ciri2}i_{sqi}}{2U_{dci}}\Delta f_2\\&+\frac{3}{2U_{dci}}\Delta i_{sqi}(U_{cqi}-wL_ii_{sdi}+k_{pi8}i_{sqi})-\frac{3k_{ii8}i_{sqi}}{2U_{dci}}\Delta z_{i8}\\&-\left[\frac{3(U_{cdi}i_{sdi}+U_{cqi}i_{sqi})}{2U_{dci}^{2}}\right]\Delta U_{dci}-\Delta i_{dci}\end{aligned}, \tag{B1c}$$

$$\frac{d\Delta\theta}{dt} = 2\pi\Delta f - w\Delta\theta \,. \quad \text{(B1d)}$$

The arguments $z_{i5} = \int (U_{sdi}^{*} - U_{sdi})$, $z_{i6} = \int (U_{sqi}^{*} - U_{sqi})$, $z_{i7} = \int (i_{sdi}^{*} - i_{sdi})$, and $z_{i8} = \int (i_{sqi}^{*} - i_{sqi})$ in B1 can be used for simplification.

REFERENCES

[1] European Network of Transmission System, "Operators for Electricity: Ten-year network development plan," 2014. *Final Repor*t, 2014.

[2] A. Bayo-Salas, J. Beerten, J. Rimez, and D. Van Hertem "Analysis of control interactions in multi-infeed VSC HVDC connections," *IET Gener, Transm. Dis.*, Vol. 10, No. 6, pp. 1336-1344, Apr. 2016.

[3] S. J. Shao and V.G. Agelidis, "Review of DC system technologies for large scale integration of wind energy systems with electricity grids," *Energies*, Vol. 3, No. 6, pp. 1303-1319, Jun. 2010.

[4] J. Dorn, H. Huang, and D. Retzmann, "A new multilevel voltage sourced converter topology for HVDC applications," *In Proc. 2008 of CIGRE*, pp. 1-8.

[5] M. P. Bahrman and B. Johnson, "The ABCs of HVDC transmission technologies," *IEEE Power Energy Mag.*, Vol. 5, No. 2, pp. 32-44, Apr. 2007.

[6] S. Cole, J. Beerten, and R. Belmans, "Generalized dynamic VSC-MTDC model for power system stability studies," *IEEE Trans. Power Syst.*, Vol. 25, No. 3, pp. 1655-1662, Sep. 2010.

[7] J. Beerten, S. D'Arco, and J. A. Suul, "Frequency-dependent cable modelling for small-signal stability analysis of VSC–HVDC systems," *IET Gener., Transm. Dis.*, Vol. 10, No. 6, pp. 1370-1381, Feb. 2016.

[8] G. O. Kalcon, G. P. Adam, O. Anaya-Lara, S. Lo, and K. Uhlen, "Small-signal stability analysis of multi-terminal VSC-based DC transmission systems," *IEEE Trans. Power Syst.*, Vol. 27, No. 4, pp. 1818-1830, Nov. 2012.

[9] L. M. Castro and E. Acha, "A unified modeling approach of multi-terminal VSC–HVDC links for dynamic simulations of large-scale power systems," *IEEE Trans. Power Syst.*, Vol. 31, No. 6, pp. 1-10, Feb. 2016.

[10] T. Ngoc-Tuan, Z. Marcus, W. Klaus, and E. István, "Generic model of MMC-VSC–HVDC for interaction study with AC power system," *IEEE Trans. Power Syst.*, Vol. 31, No. 1, pp. 27-34, Feb. 2015.

[11] J. Xu, A. M. Gole, and C. Zhao, "The use of averaged-value model of modular multilevel converter in DC grid," *IEEE Trans. Power Del.*, Vol. 30, No. 2, pp. 519-528, Apr. 2015.

[12] S. Liu, Z. Xu, W. Hua, G. Tang, and Y. L. Xue, "Electromechanical transient modelling of modular multilevel converter based multiterminal HVDC systems," *IEEE Trans. Power Syst.*, Vol. 29, No. 1, pp. 72-83, Jul. 2014.

[13] L. Zhou, S. Liu, W. Lu, and S. Hu, "Quasi-steady-state large-signal modelling of DC–DC switching converter: justification and application for varying operating conditions," *IET Power Electron.*, Vol. 7, No. 10, pp. 2455-2464, Oct. 2014.

[14] S. Chiniforoosh, J. Jatskevich, A. Yazdani, V. Sood, V. Dinavahi, J. A. Martinez, and A. Ramirez, "Definitions and applications of dynamic average models for analysis of power systems," *IEEE Trans. Power Del.*, Vol. 25, No. 4, pp. 2655-2669, Nov. 2010.

[15] S. Chandrasekar and R. Gokaraju, "Dynamic phasor modeling of type 3 DFIG wind generators (including SSCI phenomenon) for short-circuit calculations," *IEEE Trans. Power Del.*, Vol. 30, No. 2, pp. 887-897, Apr. 2015.

[16] A. Emadi, "Modeling of power electronics loads in AC distribution systems using the generalized state-space averaging method," *IEEE Trans. Ind. Electron.*, Vol. 51, No. 5, pp. 992-1000, Nov. 2004.

[17] A. M. Stankovic, R. Seth, and T. Aydin, "Dynamic phasors in modelling and analysis of unbalanced polyphase AC Machines," *IEEE Trans. Energy Convers.*, Vol.17, No. 1, pp. 107-113, Apr. 2002.

[18] P. C. Stefanov and A. M. Stankovic, "Modeling of UPFC operation under unbalanced conditions with dynamic phasors," *IEEE Trans. Power Syst.*, Vol. 17, No. 2, pp. 395-403, Apr. 2002.

[19] X. Guo, Z. Lu, B. Wang, X. Sun, L. Wang, and J. M. Guerrero, "Dynamic phasors-based modeling and stability analysis of droop-controlled inverters for microgrid applications," *IEEE Trans. Smart Grid*, Vol. 5, No. 6, pp. 2980-2987, Nov. 2014.

[20] L. Tan, A. M. Gole, and C. Zhao, "Harmonic instability in MMC–HVDC converters resulting from internal dynamics," *IEEE Trans. Power Del.*, Vol. 31, No. 4, pp. 1738-1747, Aug. 2016

[21] D. Jovcic and F. A. Jamshidi, "Phasor model of modular multilevel converter with circulating current suppression control," *IEEE Trans. Power Del.*, Vol. 30, No. 4, pp. 1889-1897, Aug. 2015.

[22] M. Daryabak, S. Filizadeh, J. Jatskevich, A. Davoudi, M. Saeedifard, V. Sood, Juan. Martinez, D. Aliprantis, J. Cano, and A. Mehrizi-Sani, "Modeling of LCC-HVDC systems using dynamic phasors," *IEEE Trans. Power Del.*, Vol. 29, No. 4, pp. 1989-1998, Aug. 2014.

[23] M. Saeedifard and R. Iravani, "Dynamic performance of a modular multilevel back-to-back HVDC system," *IEEE Trans. Power Del.*, Vol. 25, No. 4, pp. 2903-2912, Nov. 2010.

[24] Q. Song, W. Liu, and X. Li, "A steady-state analysis method for a modular multilevel converter," *IEEE Trans. Power Electron.*, Vol. 28, No. 8, pp. 3702-3713, Aug. 2013.

[25] L. Zhang, L. Harnefors, and H. P. Nee, "Interconnection of two very weak AC systems by VSC–HVDC links using power-synchronization control," *IEEE Trans. Power Syst.*, Vol. 26, No. 1, pp. 344-355, Mar. 2011.

[26] J. Zhou, H. Ding, S. Fan, Y. Zhang, and A. M. Gole, "Impact of short-circuit ratio and phase-locked loop parameters on the small-signal behavior of a VSC–HVDC Converter," *IEEE Trans. Power Del.*, Vol. 29, No. 5, pp. 2287-2296, Oct. 2014.

[27] S. R. Sanders, J. M. Noworolski, X. Z. Liu, and G. C. Verghese, "Generalized averaging method for power conversion circuits," *IEEE Trans. Power Electron.*, Vol. 6, No. 2, pp. 251-259, Apr. 1991.

[28] F. Wu, X. Zhang, K. Godfrey, and P. Ju, "Small signal

stability analysis and optimal control of a wind turbine with doubly fed induction generator," *IET Gener., Transm. Dis.*, Vol. 1, No. 5, pp. 751-760, Sep. 2007.
[29] P. Kundur, *Power System Stability and Control*, 2nd ed., McGraw-Hill, pp. 700-706, 2001.

Pan Hu (S'14) was born in Wuhan, Hubei Province, China, on August 18, 1989. He received his B.E. degree in electrical engineering from Wuhan Textile University, China, in 2012. Presently, he is pursuing a Ph.D. degree at Wuhan University. His current research interests include power system stability analysis and control and renewable energy planning.

Hongkun Chen (M'14) was born in Huanggang, Hubei Province, China, on December 13, 1967. He received his B.E. and M.E. degrees in electrical engineering from Xi'an Jiao Tong University, China, in 1988 and 1990, respectively, and his Ph.D. degree from Wuhan University, China, in 1998. From 2000 to 2003, he worked at Post-Doctoral Scientific Research in the School of Electrical Engineering, Osaka University. He is currently the vice president of the School of Electrical Engineering, Wuhan University. His research interests include power system stability analysis, power quality assessment and mitigation, and active distribution network planning.

Lei Chen (M'12) was born in Jingzhou City, Hubei Province, China, in 1982. He received his B.S. and Ph.D. degrees from the School of Electrical and Electronic Engineering, Huazhong University of Science and Technology, Hubei, in 2004 and 2010, both in electrical engineering. From 2011 to 2013, he worked at the Post-Doctoral Scientific Research Workstation of Hubei Electric Power Company. Since 2013, he has been a teacher in the School of Electrical Engineering, Wuhan University. His research interests include power system real-time simulation, smart grids, and superconducting power applications.

Xiaohang Zhu (S'16) was born in Yichang City, Hubei Province, China, in 1992. He received his B.S. degree from Huazhong University of Science and Technology, Wuhan, China, in 2015. He is now pursuing his master's degree in the School of Electrical Engineering, Wuhan University, China. His current research interests are small-signal stability in power systems and power quality improvement.

Xuechun Wang was born in Jingzhou City, Hubei Province, China, in 1994. She received her B.S. degree from Wuhan University, Wuhan, China, in 2015. She is now pursuing her master's degree in the School of Electrical Engineering, Wuhan University, China. Her current research interests are operation and management in power systems, active distribution network planning, and stability analysis.